Electronic Supplementary Material (ESI) for Journal of Materials Chemistry A.

Supporting information

Efficient TeO_2/Ag transparent top electrode for 20%-efficiency bifacial perovskite solar cells with a bifaciality factor exceeding 80%

Dazheng Chen*†, Shangzheng Pang†, Long Zhou†, Xueyi Li, Aixue Su, Weidong Zhu, Jingjing Chang, Jincheng Zhang, Chunfu Zhang*, and Yue Hao

Wide Bandgap Semiconductor Technology Disciplines State Key Laboratory, School of Microelectronics, Xidian University, Xi'an 710071, China

Shaanxi Joint Key Laboratory of Graphene, Xidian University, Xi'an, 710071.

*Corresponding author

E-mail addresses: dzchen@xidian.edu.cn, cfzhang@xidian.edu.cn

Three authors have equally contributed to this study.

1. Method

1.1 Materials

Methylammonium iodide (MAI, 99.8%), Formamidinium iodide (FAI, 99.8%), and phenylethylammonium iodide (PEAI) were acquired from Dyesol. Lead iodide (PbI_2, 99.999%) and Lead chloride ($PbCl_2$, 99.999%), Bathocuproine (BCP, 96%), Chlorobenzene (CB, 99.8%), isopropanol (IPA, 99.5%), and N,N'-Dimethylformamide (DMF, 99.8%) were provided from Sigma. Phenyl-C_{61}-butyric acid methyl ester (PCBM, 98%) was purchased acquired from Nano-C. Silver (Ag) and Tellurium oxide (TeO_2, 99.99%) were acquired from Zhongnuo new material and Alfa, respectively. All the materials were used without further purification. All the materials were used without further purification.

1.2 Theoretical calculations

In the optical calculation, the TMF method[1-5] was used as an optical model to calculate the carrier generation rate (G). Here, only light at normal incidence to the substrate is considered for photovoltaic devices. It is assumed that every layer is flat and homogenous, and the absorbed photons could completely converted to free charges, which are collected by the electrodes.

We have performed calculations with two subsets of 2x2 matrices. The perovskite solar cell consists of a stack of m thin-film layers, each of which (j) is described by its complex index of refraction $\tilde{n}_j=\eta_j+ik_j$ and thickness d_j, sandwiched between air and a semi-infinite substrate. All the n and k values have been taken from websites and references[6-9] Light is incident on the substrate from the left. The optical electric field

of light traveling to the right is denoted as E^+; that traveling left as E^-. The substrate and air at the back of the device are treated as layers 0 and m+1, respectively. The behavior of light at the interface between layer *j* and layer *k* can be described by the interface matrix I_{jk}, which for normal incidence can be given in the simplified form:

$$I_{jk} = \begin{bmatrix} (\tilde{n}_j + \tilde{n}_k)/2\tilde{n}_j & (\tilde{n}_j - \tilde{n}_k)/2\tilde{n}_j \\ (\tilde{n}_j - \tilde{n}_k)/2\tilde{n}_j & (\tilde{n}_j + \tilde{n}_k)/2\tilde{n}_j \end{bmatrix} \tag{1}$$

Similarly, the effect on the optical electric field from propagating through each layer is described by the layer matrix L_j:

$$L_j = \begin{bmatrix} e^{-i\xi_j d_j} & 0 \\ 0 & e^{i\xi_j d_j} \end{bmatrix} \tag{2}$$

where $\xi_j = 2\pi\tilde{n}_j / \lambda$ and λ the wavelength of light. The optical electric field in the substrate (subscript 0) is related to that in the atmosphere (subscript m+1) by the total transfer matrix S

$$\begin{bmatrix} E_0^+ \\ E_0^- \end{bmatrix} = S \begin{bmatrix} E_{m+1}^+ \\ E_{m+1}^- \end{bmatrix} \tag{3}$$

where S is the product of all the interface and layer matrices

$$S = \begin{bmatrix} S_{11} & S_{12} \\ S_{21} & S_{22} \end{bmatrix} = \left(\prod_{v=1}^{m} I_{(v-1)v} L_v \right) \cdot I_{m(m+1)} \tag{4}$$

The optical electric field at a distance x within layer j can be expressed as

$$E_j(x) = E_j^+(x) + E_j^-(x) \tag{5}$$

To express $E_j(x)$ in terms of known quantities, eq.(4) is split into two partial transfer matrices by the relation $S = S_j' L_j S_j''$. These two matrices are separately expressed as

$$S_j' = \begin{bmatrix} S_{j11}' & S_{j12}' \\ S_{j21}' & S_{j22}' \end{bmatrix} = \left(\prod_{v=1}^{j-1} I_{(v-1)v} L_v \right) \cdot I_{(j-1)j} \tag{6}$$

$$S_j^{''} = \begin{bmatrix} S_{j11}^{''} & S_{j12}^{''} \\ S_{j21}^{''} & S_{j22}^{''} \end{bmatrix} = \left(\prod_{v=j+1}^{m} I_{(v-1)v} L_v \right) \cdot I_{m(m+1)} \tag{7}$$

After algebraic manipulation, eq. (5) can be expressed as

$$E_j(x) = \left[t_j^{+} e^{i\xi_j x} + t_j^{-} e^{-i\xi_j x} \right] E_0^{+} \tag{8}$$

where E_0^{+} is the optical electric field inside the substrate incident on layer 1, and

$$t_j^{+} = [S_{j11}^{'} + S_{j12}^{'} r_j^{''} e^{i2\xi_j d_j}]^{-1} \tag{8}$$

$$r_j^{''} = S_{j21}^{''} / S_{j11}^{''} \tag{10}$$

To obtain quantitatively accurate results for the intensity in each layer, the effect of the substrate is included by summing the intensities within the glass as opposed to the optical electric field. The intensity of light incident on the multilayer from within the substrate I_S is then expressed as

$$I_S = I_0 \frac{T_S e^{-\alpha_s d_s}}{1 - R R_S e^{-2\alpha_s d_s}} = I_0 T_{\text{int}} \tag{11}$$

where I_0 is the light intensity incident on the solar cell, R and T are the reflectance and transmittance of the stack, respectively, and variables with the subscript S represent values of the substrate. The internal transmittance T_{int} for the substrate is defined in terms of the absorption coefficient $\alpha_j = 4\pi k_j / \lambda$. By combining eqs. (8) and (11), the light intensity in layer j at position x can be expressed as

$$I_j(x) = I_0 T_{\text{int}} \left| t_j^{+} \right|^2 \frac{n_j}{n_s} \left[e^{-\alpha_j x} + \rho_j^{''2} e^{-\alpha_j (2d_j - x)} + 2\rho_j^{''} e^{-\alpha_j d_j} \cos\left(\frac{4\pi\eta_j}{\lambda} (d_j - x) + \delta_j^{''} \right) \right] \tag{12}$$

where $\rho_j^{''}$ and $\delta_j^{''}$ are the argument and phase of the quantity in eq. (10), respectively. Once the distribution of the light intensity is determined, the energy flow dissipation per second for a single wavelength in layer j at position x, Q, is given as

$$Q_j(x,\lambda) = \alpha_j(\lambda) I_j(x,\lambda) \tag{13}$$

Then, the absorption rate in layer j can be expressed as

$$N_j(x) = \int_{300nm}^{800nm} Q_j(x, \lambda) \frac{\lambda}{hc} d\lambda \quad (14)$$

where $N_j(x)$ represents the number of photons absorbed in layer *j* per unit area, time, and propagation length, hc/λ is the photon energy at a specified wavelength λ, h is the Planck constant, and c is the speed of light in vacuum. From the obtained N, the carriers generation rate G could be obtained.

For the electrical properties, the Shockley–Read–Hall (SRH) recombination, radiative recombination, and Auger recombination models were considered in the PSC. The standard AM 1.5G solar spectrum was used to get current density-voltage (J-V) curve under illumination. Material parameters of each layer were obtained from literatures and summarized in Table S1[10-14]. The calculation is mainly based on three basic equations which are Possion's equation, carrier continuity equation and drift-diffusion equation, respectively:

Possion's equation:

$$\frac{\partial^2 \varphi}{\partial x^2} = \frac{q}{\varepsilon}(n - p) \quad (3)$$

Carrier continuity equation:

$$\frac{\partial n}{\partial t} = \frac{1}{q}\frac{\partial J_n}{\partial x} + G - R \qquad \frac{\partial p}{\partial t} = -\frac{1}{q}\frac{\partial J_p}{\partial x} + G - R \quad (4)$$

Drift-diffusion equation:

$$J_n = qD_n\frac{\partial n}{\partial x} - q\mu_n n\frac{\partial \varphi}{\partial x} \quad J_p = -qD_p\frac{\partial p}{\partial x} - q\mu_p p\frac{\partial \varphi}{\partial x} \quad (5)$$

Where φ is electric potential, ε is dielectric constant, q is electron charge, n is electron concentration, p is hole concentration, J_n is electron current density, J_p is hole

current density, G is carriers generation rate, R is carriers recombination rate, D_n is electron diffusion coefficient, D_p is hole diffusion coefficient, μ_n is electron mobility, μ_p is hole mobility.

Table S1. The parameters used in the calculation with the Silvaco software.

Parameters	**NiO**	**CH3NH3PbI3**	**PCBM**
Thickness（nm）	40	500	45
Eg(eV)	3.76	1.57	2.2
Permittivity	11.75	30	4
Affinity(eV)	1.44	3.93	4
Nc(cm^{-3})	2.5e20	1e20	2.5e20
Nv(cm^{-3})	2.5e20	1e20	2.5e20
Mun($cm^2 V^{-1} s^{-1}$)	0.01	50	0.01
Mup($cm^2 V^{-1} s^{-1}$)	0.01	50	0.01

1.3 Device fabrication

Bifacial PSCs were fabricated on ITO-coated glass substrates (2×2.5 cm^2, 10 Ω/□). The substrates were ultrasonically cleaned with detergent, de-ionized water, acetone, and alcohol at 50 ℃ for 20 min. Then they were treated in a UV-ozone oven for 15 min. A thin layer of NiO_x was spin-coated on the substrates at 3000 rpm for 30s and annealed at 250 ℃ for 45 min. After that, the substrates were transferred into a glove box filled with nitrogen. The PbX_2 precursor solution was prepared by dissolving 1.36 M PbI_2 and 0.24 M $PbCl_2$ in the DMF and stirring for 2 h at 72 ℃. 100 mg MAI:FAI (7:3 mass. ratio) were dissolved in the 1mL IPA mixed with 1.0 vol% DMF to be the clear MAI:FAI precursor solution. For the two step solution method, the PbX_2

precursor solution was spin-coated on the top of the NiOx/ITO/Galss samples at 3000 rpm for 45 s, following the spinning of MAI:FAI at 3000 rpm for 45 s, and then all samples were annealed on the hotplate at 100 ℃ for 10 min under the IPA atmosphere to form the perovskite layer. PEAI and MAI dissolved in IPA with 0.9 vol % DMF were spin-coated on the pervoskites layer and annealed at 100 ℃ for 5 min, which could further suppressed trap density. Next, the PCBM (20 mg/ml in chlorobenzene) and BCP (0.5 mg/ml in IPA) was sequentially spin-coated on the perovskite layer at 2000 rpm for 45s and 6000 rpm for 45s. After that, a layer of Ag (11 nm) and TeO_2 (20, 40, 50 nm) were thermally evaporated on the BCP layer sequentially to finished the device fabrications. The thicknesses of Ag and TeO_2 were estimated in situ with a calibrated quartz crystal monitor. The devices have the active area of 0.07 cm^2 and 1 cm^2 defined by shadow masks. All the materials were used without further purification(seeing supporting information).

1.4 Device characterization

The photovoltaic performances of bifaical PSCs were measured by the Keithley 2400 source meter under the simulated AM 1.5G (One sun) illumination of 1000 W/m^2 from a sunlight simulator (Sanei Electric, XES-300T1). The illumination intensity was calibrated by a reference silicon cell certificated by the National Renewable Energy Laboratory. The incident photo-to-current conversion efficiency (IPCE) of PSCs was measured by the quantum efficiency measurement system (SCS10-X150, Zolix instrument. Co. Ltd). The transmittance spectra were measured by the UV–visible spectrophotometer (Perkin-Elmer Lambda 950). The film morphology

and crystal quality were characterized by a JSM-7800F extreme-resolution analytical field emission scanning electron microscope (SEM) and X-ray diffractormeter (D8 Advance, Bruker, Germany). All the measurements were performed at room temperature under ambient atmosphere.

2. Experimental Results

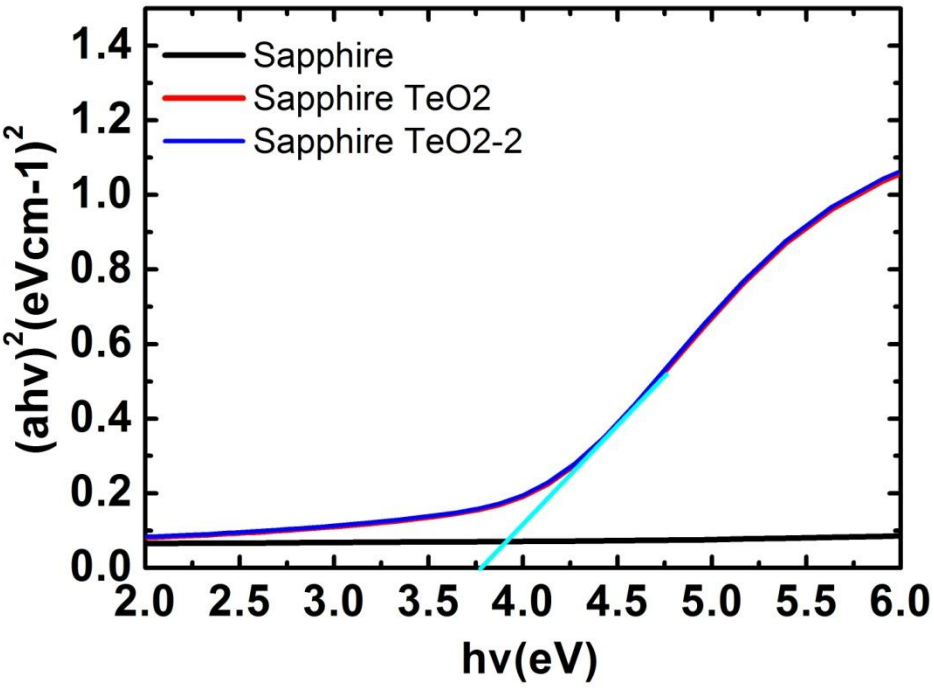

Fig. S1 Absorption coefficient as a function of photon energy for sapphire (Al_2O_3) substrate and two TeO_2/sapphire samples. The extracted optical bandgap of TeO_2 is about 3.80 eV, which is close to the reported optical band gap of 3.76 eV and 3.50 eV for amorphous and single crystal TeO_2[15].

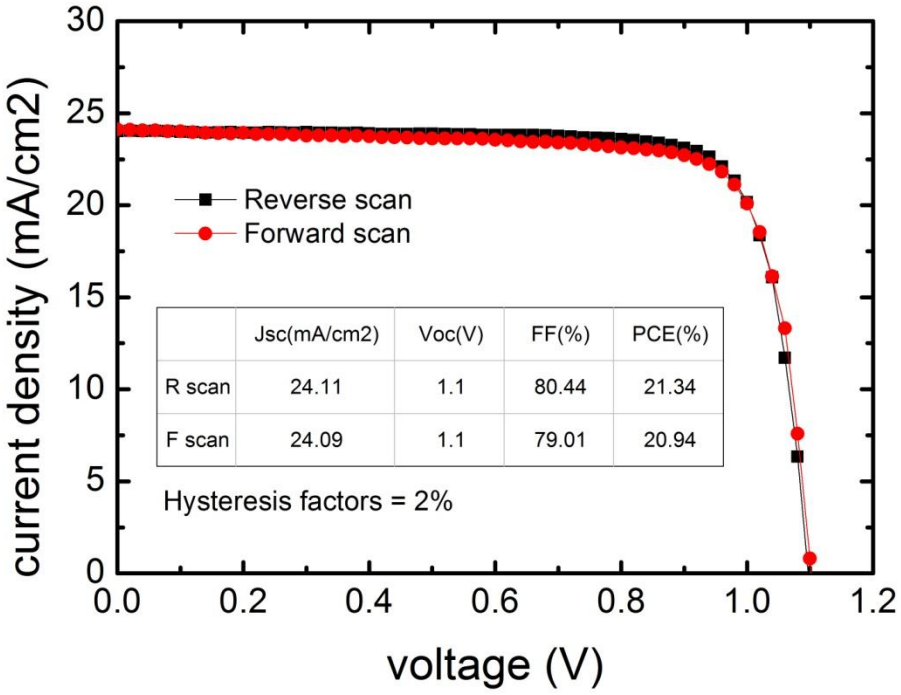

Fig. S2 JV characteristics of ITO based reference PSC (Device E). The calculated hysteresis factors of Device E is about 2%.

3. Calculation results

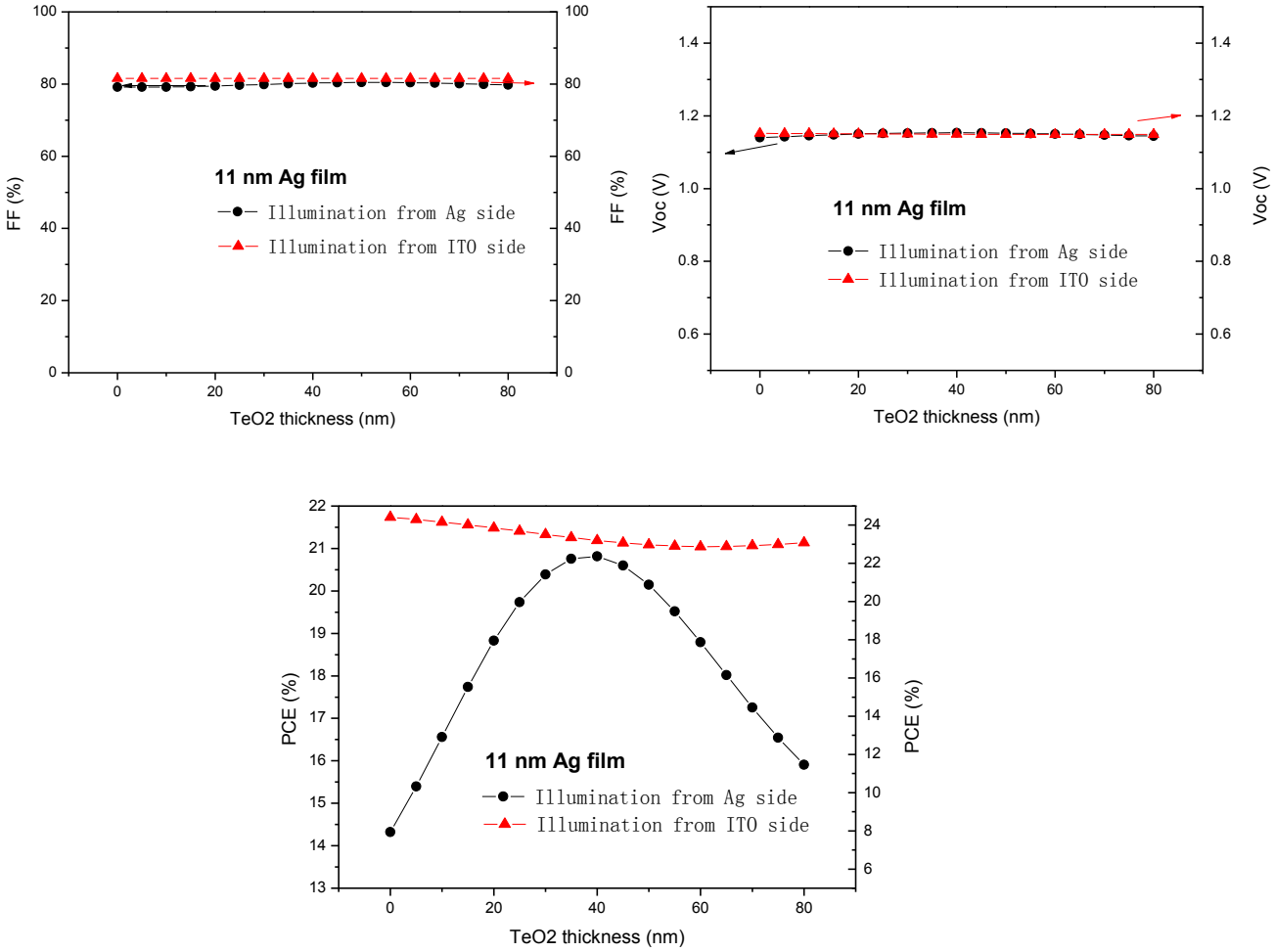

Fig. S3 Simulated PCE, FF, Voc for bifacial PSCs with TeO_2(0-80nm)/Ag(11 nm) top electrode.

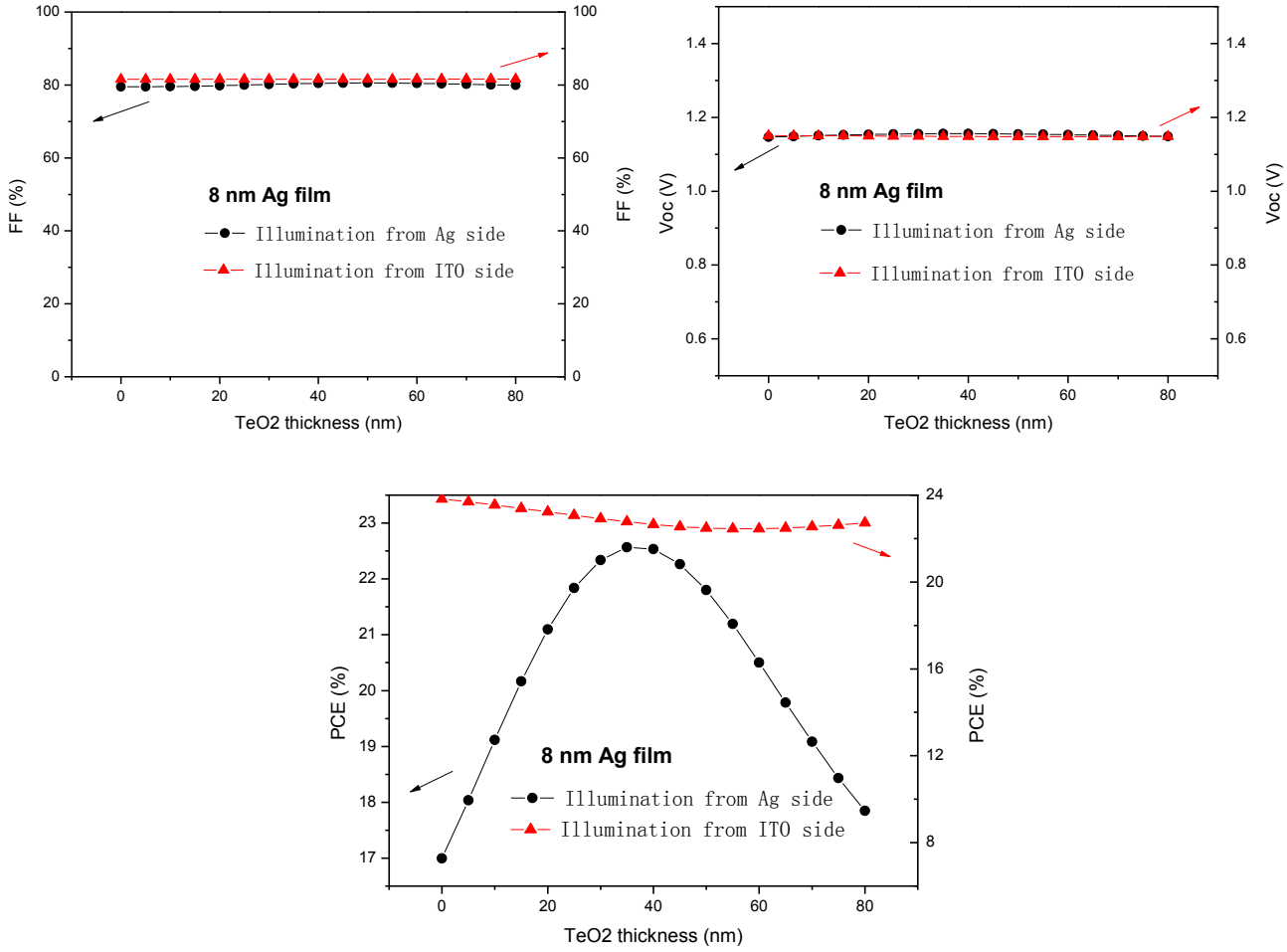

Fig. S4 Simulated PCE, FF, Voc for bifacial PSCs with TeO_2(0-80nm)/Ag(11 nm) top electrode.

References

[1] L. A. A. Pettersson, L. S. Roman, and O. Inganas, J. Appl. Phys., 1999, 86, 487-496.

[2] Y. Long, Appl. Phys. Lett., 2009, 95, 193301.

[3] Y. Long, Sol. Energy Mater. Sol. Cells, 2011, 95, 3400–3407.

[4] G. F. Burkhard , E. T. Hoke , and M. D. McGehee, Adv. Mater., 2010, 22, 3293–3297.

[5] Z. Wang, C. Zhang, D. Chen, J. Zhang, Q. Feng, S. Xu, X. Zhou, and Y. Hao, Jpn. J. Appl. Phys., 2012, 51, 122301.

[6] J. Huang, C. Li, C. Chueh, S. Liu, J. Yu, and A. K. Y. Jen, Adv. Energy Mater., 2015, 5, 1500406.

[7] P. Löper et al. J. Phys. Chem. C, 2014, 6, 66–71.

[8] [Online]. Available: https://www2.pvlighthouse.com.au/resources/photovoltaic%20materials/refractive%20index/refractive%20index.aspx

[9] D. Chen, H. Xi, C. Zhang, J. Chang, Z. Lin, W. Zhu, S. Pang, H. Yang, J. Zhang, L. Guo, Y. Hao, IEEE Photonics Journal, 2018, 10, 8400209.

[10] L. Hu, J. Peng, W. Wang , Z. Xia, J. Yuan, J. Lu, X. Huang, W. Ma, H. Song, W. Chen, Y.B. Cheng, J. Tang, ACS Photonics, 2014. 1, 547–553.

[11] O. Malinkiewicz, A. Yella, Y.H. Lee, G.M. Espallargas, M. Graetzel, M.K. Nazeeruddin, H.J. Bolink, Nat. Photon., 2013. 8, 128–132.

[12] Minemoto, T., Murata, M., 2016. (SCAPS), 054505.

[13] H. Tsai, W. Nie, J.-C. Blancon, C.C. Stoumpos, R. Asadpour, B. Harutyunyan, A.J. Neukirch, et al. Nature, 2016, 536, 312–316.

[14] F. Shan, A. Liu, H. Zhu, W. Kong, J. Liu, B. Shin, E. Fortunato, R. Martins, G. Liu, J. Mater. Chem. C, 2013, 1, 5837.

[15] R. Nayak, V. Gupta, A. L. Dawar and K. Sreenivas, *Thin Solid Films*, 2003, 445, 118–126.